

## Implications of Small-Scale Flow Features to Modeling Dispersion over Complex Terrain

R. M. BANTA AND L. D. OLIVIER

*Environmental Technology Laboratory, NOAA/ERL, Boulder, Colorado*

P. H. GUDIKSEN AND R. LANGE

*Lawrence Livermore National Laboratory, Livermore, California*

(Manuscript received 6 March 1995, in final form 24 August 1995)

### ABSTRACT

Small-scale, topographically forced wind systems often have a strong influence on flow over complex terrain. A problem is that these systems are very difficult to measure, because of their limited spatial and temporal extent. They can be important, however, in the atmospheric transport of hazardous materials. For example, a nocturnal exit jet—a narrow stream of cold air—which flowed from Eldorado Canyon at the interface between the Rocky Mountains and the Colorado plains near the Rocky Flats Plant (RFP), swept over RFP for about 3 h in the middle of the night of 4–5 February 1991. It extended in depth from a few tens of meters to approximately 800 m above the ground. Because the jet was so narrow (2 km wide), it was poorly sampled by the meteorological surface mesonet, but it did prove to have an effect on the dispersion of tracer material released from RFP, producing a secondary peak in measured concentration to the southeast of RFP. The existence and behavior of the jet was documented by Environmental Technology Laboratory's Doppler lidar system, a scanning, active remote-sensing system that provides fine-resolution wind measurements. The lidar was deployed as a part of a wintertime study of flow and dispersion in the RFP vicinity during February 1993.

The MATHEW-ADPIC atmospheric dispersion model was run using the case study data from this night. It consists of three major modules: an interpolation scheme; MATHEW, a diagnostic wind-flow algorithm that calculates a mass-consistent interpolated flow; and ADPIC, a diffusion algorithm. The model did an adequate job of representing the main lobe of the tracer transport, but the secondary lobe resulting from the Eldorado Canyon exit jet was absent from the model result. Because the jet was not adequately represented in the input data, it did not appear in the modeled wind field. Thus, the effects of the jet on the transport of tracer material were not properly simulated by the diagnostic model.

### 1. Introduction

Those familiar with observations of 3D wind fields over complex terrain are certainly aware that highly localized, organized atmospheric features can strongly affect the low-level flow. Because of the limited extent of these features in time and space, however, few documented cases of their nature, structure, and behavior exist. Such features obviously influence the transport of atmospheric contaminants, but the nature and magnitude of the effects is poorly understood. They also affect one's ability to model accurately this transport over complex terrain.

Dispersion of atmospheric contaminants is computed using models of varying complexity. It is often modeled as a combination of advection of the contaminants plus their diffusion. Advection is calculated using a mean wind field that may be determined by a diagnostic

model, for example, which interpolates (and extrapolates) among wind observations. Diffusion is determined by a diffusion algorithm that may be as simple as a Gaussian plume or puff, or as complex as a fully stochastic representation, as, for example, a Markov process.

Determining the fate of hazardous materials released into the atmosphere is an important application for atmospheric modeling. It is crucial to understand how well models perform, and especially under what conditions they are apt to produce errors. In complex terrain the accuracy of the dispersion calculation depends critically on the accuracy of the modeled wind field. As Mikkelsen and Desiato (1993) and Hunt et al. (1991) have pointed out, "over complex terrain, simulation of atmospheric diffusion is mainly limited by the capabilities of the flow models." But the advecting wind field produced by a diagnostic model is "no more accurate than the observations used," and, "if significant flow features, such as jets, occur between measurement sites, the predicted transport could be seriously in error" (Banta et al. 1993b). Unfortunately, in complex terrain the advection field often is "seriously

---

Corresponding author address: Robert M. Banta, NOAA/ERL (R/E/ET2), 325 Broadway, Boulder CO 80303-3328.  
E-mail: rbanta@etl.noaa.gov

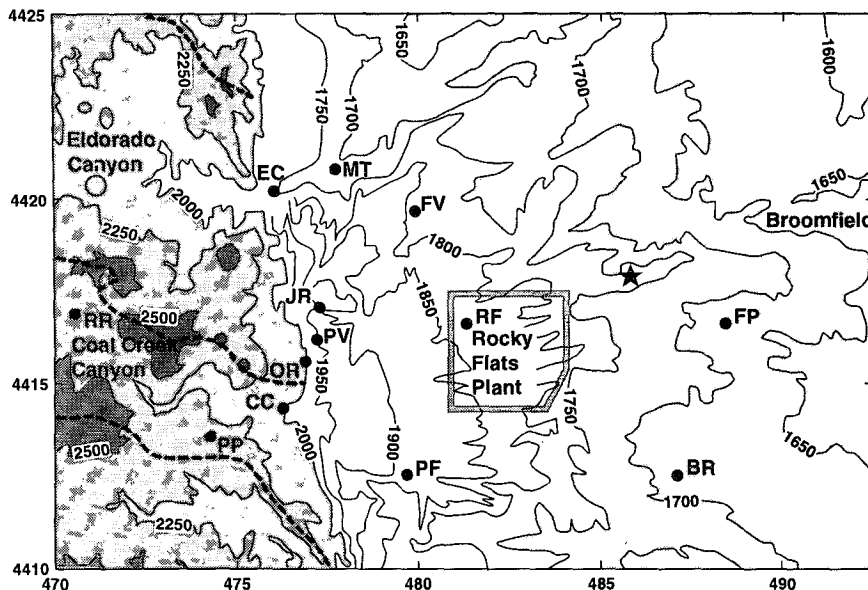


FIG. 1. Contour map of Rocky Flats Plant vicinity, showing the locations of instrumentation sites. Vertical and horizontal axes are UTM (universal transverse Mercator) coordinates in kilometers. Star indicates the location of the Doppler lidar, EC is the tethersonde site at the mouth of Eldorado Canyon, CC is the minisodar and surface station site at the mouth of Coal Creek Canyon, and RF is the location of the Rocky Flats tower and rawinsonde ascents. Location PV was a tethersonde site, FP an airsonde site, and MT and FV were alternate sites for the Eldorado Canyon tethersonde if the winds were too strong at EC. The other two-letter designators were surface mesonet locations. Contours (MSL) are at intervals of 50 m over the plains, and 250 m over the mountains (above 2000 m). Regions over 2250 m are shaded medium, and over 2500 m, shaded darkly. The heavy dashed lines in the mountains represent the ridge high points, indicating the divides between the watersheds (airsheds) for each stream flowing out of the mountains.

in error” because of spatial nonrepresentativeness of the observations used to generate the wind field and other sampling errors in space and time.

The implication of this inaccuracy to the selection of appropriate models for use in complex terrain is that simple schemes perform about as well as sophisticated diagnostic interpolation models under these conditions. Thus, there is currently little reason to use more sophisticated models for routine applications, and simpler, cruder models, such as the Gaussian plume, are retained. At the other end of the complexity spectrum, fully prognostic, dynamic models show promise, but they are expensive to run and use excessive run times for operational use at present.

In the following study we document a small-scale flow feature, a nocturnal canyon exit jet, that became prominent in the low-level flow field over the Rocky Flats Plant (RFP) just east of the Front Range of the Rocky Mountains in Colorado. The finescale structure and behavior of this feature were revealed by a scanning Doppler lidar operated on the plains near RFP by the Environmental Technology Laboratory (ETL) of the National Oceanic and Atmospheric Administration’s Environmental Research Laboratories (NOAA/ERL). We address three major questions: 1) What was the spatial structure of the jet and how did it evolve in

time? 2) What influence did the jet have on low-level dispersion in the vicinity of RFP? 3) What are the implications to the accuracy of the diagnostic modeling of dispersion in this region? Canyon exit jets in other regions have been described by Whiteman (1990) and Filliger and Wanner (1986).

## 2. Topography, instrumentation, and synoptic/ large-scale conditions

### a. Topography

A field experiment was conducted during January and February 1991 in the vicinity of the Rocky Flats Plant to study the effects of the complex topography on wind flows and atmospheric transport of material released from RFP. The experiment was a part of the Atmospheric Studies in Complex Terrain (ASCOT) project. Further details on the purpose and instrumentation of the project are given in section 2c and by Elderkin and Gudiksen (1993) and Doran (1993).

The Rocky Flats Plant is located approximately 25 km northwest of Denver, Colorado, and 6 km east of the foothills of the Rocky Mountains, on 385 acres of rolling terrain (Fig. 1). Terrain in the vicinity of RFP ranges from hills and gullies to the north, south, and

east, to the ascent of the north-south Front Range of the Rocky Mountains on the west. Two canyons that drain from the mountains to the plains, Coal Creek and Eldorado, significantly influence the flow over Rocky Flats, and the South Platte River valley drains northward about 20 km to the east of RFP. The ridge that forms the Continental Divide, 40 km to the west of RFP, also affects the flow along the Front Range of Colorado. Many communities are located within a few kilometers of RFP, magnifying the importance of understanding the transport and diffusion of hazardous materials in the RFP region.

### b. Doppler lidar

#### 1) CHARACTERISTICS

ETL's Doppler lidar, an active remote sensing instrument that measures wind velocity and backscattered signal intensity, has been described by Post and Cupp (1990). It transmits pulses of eye-safe infrared (IR) light with a wavelength of 10.59  $\mu\text{m}$ . Atmospheric aerosols, mostly in the 1–3- $\mu\text{m}$ -radius size range, scatter a small fraction of this IR back to the lidar. Two kinds of information are measured, the backscattered intensity and the frequency of the return signal. The backscatter is an indication of the concentration of aerosols in the air, but it is a complicated function of the size, shape, concentration, and composition of the aerosols, and the amount of moisture in the intervening air. From the Doppler shift of the returned frequency, the radial velocity  $u_r$ , or the velocity along the beam, can be calculated. Table 1 lists the general characteristics of the lidar during the RFP experiment.

Two other important characteristics, a narrow beam and the absence of antenna sidelobes, result from the lidar transmitting its beam through a telescope rather than through an antenna, as, for example, a radar does. These characteristics are a great advantage for scanning into complex terrain because the flow can be measured very close to the terrain surface. The ETL Doppler lidar can complete a full 360° scan in azimuth in less than 2 min, or 180° in elevation or azimuth in less than 1 min. A real-time color display in the lidar trailer allows for the tailoring of measurements to meteorological conditions while the experiment is in progress. Recently the lidar has been used to study a sea breeze (Banta et al. 1993a), a prescribed forest fire (Banta et al. 1992), severe downslope windstorms (Clark et al. 1994; Neiman et al. 1988), and flow in the Grand Canyon (Banta et al. 1991).

#### 2) PRINCIPAL SCANS PERFORMED

One of the most useful scans for wind analysis taken during the experiment was a high-resolution, horizontal "raster" or volume scan. The lidar obtained measurements from south of Coal Creek Canyon to north of Eldorado Canyon by scanning from 225° to 305° in

TABLE 1. Lidar parameters for Rocky Flats.

Wavelength ( $\mu\text{m}$ )	10.59
Maximum range (km)	up to 30.00
Minimum range (km)	1.20
Range resolution (m)	300.00
Beam width ( $\mu\text{rad}$ ) [°]	90 [0.005]
Root-mean-square velocity accuracy ( $\text{cm s}^{-1}$ )	60.00
Pulse repetition frequency (Hz)	10.00
Pulses averaged	3.00

azimuth at a rate of  $2^\circ \text{ s}^{-1}$  and from  $0^\circ$  to  $5^\circ$  in elevation, incrementing every  $0.2^\circ$  (corresponding to a height increment of 35 m at a range of 10 km). The canyon flows and the upslope or downslope winds along the foothills were well documented by these scans. We attempted to take these scans approximately every 45–60 min, to capture the evolution of the canyon and slope flows.

Vertical slice scans, where the scanner remains at a constant azimuth while scanning in elevation from horizon to horizon, were also useful for the analysis of the winds in the RFP region, particularly along the axes of the canyons. The lidar's narrow beam allows for high vertical resolution during this type of scan, and the vertical structure of the wind flow and aerosol layers were well documented during the experiment. In addition to taking measurements in the canyons, vertical slice scans were performed at intervals around the compass, offering information about the wind flow over the plains and additional information about the flow near the foothills.

To assess the large-scale wind flow near the ground and aloft, conical scans, in which the scanner rotates a full  $360^\circ$  in azimuth at a fixed elevation angle, were performed at elevation angles ranging from  $0^\circ$  to  $60^\circ$ . This type of scan indicates the horizontal variability of the winds. Using the VAD (velocity-azimuth display) technique (Browning and Wexler 1968), vertical profiles of the horizontal wind were calculated.

### c. Other instrumentation

Instruments from a number of laboratories participated in the RFP experiment (Elderkin and Gudiksen 1993; Banta et al. 1995). The Lawrence Livermore National Laboratory (LLNL) had eight instrumented towers located in the RFP region and a tethered sonde launched from the Coal Creek Canyon opening. All LLNL towers measured winds and temperatures, and four of them had net radiometers. Los Alamos National Laboratory (LANL) launched two-hourly rawinsondes from RFP. The Pacific Northwest Laboratory (PNL) provided a minisodar and airsondes. Argonne National Laboratory (ANL) deployed one minisodar near the entrance of Coal Creek Canyon and another at other sites near RFP, as one of the ANL minisodars was mobile and took measurements where needed. NOAA's

Atmospheric Turbulence and Diffusion Division (ATDD) launched a tethersonde from a position near the foothills, but between Coal Creek and Eldorado Canyons. Instrument locations are indicated in Fig. 1.

At the RFP site a 61-m instrumented tower operates continuously, obtaining data at three levels; 10, 25, and 60 m. All levels measure wind speed and direction, temperature, and vertical velocity. The 10-m level also measures dewpoint and precipitation. Measurements were recorded in 15-min averages.

In addition to the lidar, ETL placed five 915-MHz wind profilers on the plains and one near the Continental Divide, and operated hourly tethersondes near the mouth of Eldorado Canyon when the wind speeds were less than  $10 \text{ m s}^{-1}$ . Discussions of the profilers and their use in complex terrain have been given by Ecklund et al. (1988, 1990), Neff et al. (1991), and Wolfe et al. (1991, 1993). Two of the ETL profilers were equipped with a radio acoustic sounding system (RASS), which obtained vertical profiles of virtual temperature (May et al. 1989).

Measurements from instrumentation not connected with the ASCOT experiment include the NOAA/Forecast Systems Laboratory's (FSL) mesonet, a network of 22 surface stations ranging from the foothills to the plains, and three wind profilers at two sites, a 915 MHz at Stapleton Airport, and a 404 MHz equipped with RASS along with a 50 MHz at Platteville. Investigators in the 1991 Winter Icing and Storms Project (WISP) also obtained data during this time period, mostly during cloudy conditions (Rasmussen et al. 1992).

The tracer employed in this experiment was sulfur hexafluoride ( $\text{SF}_6$ ). It was released continuously at a constant rate for 11 h from a surface site to the east of the RFP meteorological tower starting at 2000 MST and ending at 0700 MST, as described by Shearer (1992) and Elderkin and Gudiksen (1993). The release rate was determined in two ways, which differed slightly: the mass flow controller indicated  $13.05 \text{ kg h}^{-1}$  and a technique using the weight loss of the gas cylinder during the release period indicated  $12.16 \text{ kg h}^{-1}$  (Shearer 1992). Sampling began 2 h after the start of the release and continued for 9 h, in 9 consecutive 1-h samples. Samplers were mounted approximately 1 m above the ground and arranged in two concentric rings around the release site, at radii of 8 and 16 km (Fig. 2). Spacing was every  $5^\circ$  around each ring to the extent possible. Including supplementary and redundant samplers, a total of 172 samplers was deployed. Two mobile samplers, on a van and a helicopter, chased the plume to provide a real-time estimate of its location.

*d. Synoptic conditions*

The main synoptic feature on the night of 4–5 February 1991 was a surface high pressure system centered over the Colorado–Utah border. This high pressure

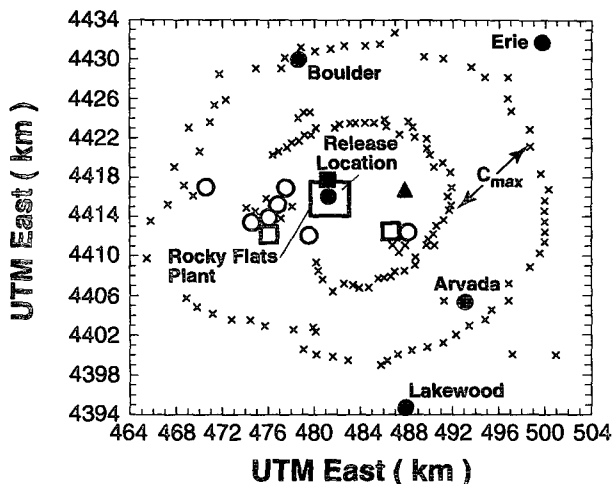


FIG. 2. Map showing the location of the surface tracer sampling network around RFP. Samplers are indicated by the small crosses, open circles represent surface mesonet sites, closed circles are FSL mesonet sites, and the solid square and triangle are the locations of upper-air balloon ascents. Vertical and horizontal coordinates are in kilometers; “ $C_{max}$ ” indicates the location of the sampler in each ring where the maximum concentration was measured for the time period of this study, as described in the text.

system remained nearly stationary throughout the night, and the weak synoptic forcing over Colorado allowed thermally forced drainage flows to form. The 50-kPa analysis at 0000 UTC 5 February indicated that the ridge aloft was continuing to build, and slight warm advection occurred at 70 and 50 kPa. Denver NWS soundings indicated westerly winds at 70 kPa and northwesterly winds at 50 kPa. Surface winds were relatively light and variable throughout the night, except where dominated by canyon drainage. Lidar measurements of surface wind flow showed that early in the evening (1900 MST, 0200 UTC) the surface winds were southwesterly to southerly. The surface winds backed with time to easterly by 0000 MST, and then shallow northerly winds appeared by 0200 MST. By 0500 MST the surface winds were southerly again.

*e. Diffusion and transport model description*

The dispersion model used in this study consisted of three parts, a 3D interpolation algorithm, the MATHEW diagnostic mass-conservation scheme, and the ADPIC turbulent diffusion model, which uses the MATHEW output as the mean wind input about which the turbulence fluctuates. Input for the 3D interpolation scheme consists of surface mesonet data, one or more vertical wind profiles, and digitized topography data. The wind at each grid point is interpolated from the three nearest measurement stations for each level using a  $1/r^2$  weighting factor as described by Sherman (1978), where  $r$  is the distance from the grid point to the measurement point. The MATHEW model (Sher-

man 1978) employs a variational method to assure that the three-dimensional gridded mean wind field is mass conservative. Wind fields are generated for each hour and assumed to persist until the next hour.

ADPIC (Lange 1978, 1985, 1989, 1992) is a three-dimensional, numerical diffusion and transport model capable of simulating the time- and space-varying dispersal of atmospheric contaminants under complex-terrain conditions Sullivan et al. (1993). It is a particle-in-cell model in which Lagrangian "mass" particles are transported inside a fixed grid. ADPIC provides a flexible framework for the diffusion calculation, capable of using many different diffusion schemes. For example, Lange (1993) compared results from a gradient-transport method with the same run using a stochastic Markov chain (Monte Carlo) method employing the Langevin equation. Elderkin and Gudiksen (1993) compared diffusion model results from several different models for the present case.

The present study employs the Langevin model introduced by Lange (1993). It consists of a pair of stochastic differential equations that describe the trajectories of "marked" particles. In the vertical dimension, these are

$$dw = \left[ - \left( \frac{C_0 \epsilon}{2\sigma_w^2} \right) w + \frac{1}{2} \left( 1 + \frac{w^2}{\sigma_w^2} \right) \frac{\partial \sigma_w^2}{\partial z} \right] dt + (C_0 \epsilon)^{1/2} dW(t) \quad (1a)$$

and

$$dz = w dt. \quad (1b)$$

Here  $w$  is the vertical Lagrangian velocity,  $\sigma_w^2$  is the variance of  $w$ ,  $\epsilon$  is the mean rate of dissipation of turbulence kinetic energy,  $C_0$  is a universal constant,  $dW(t)$  is a Gaussian distributed random number with mean of zero and variance  $(dt)^{1/2}$ , and  $dz$  is the distance a particle will travel in the time increment  $dt$ . The  $dt$  term in Eq. (1a) is deterministic and the  $dW(t)$  term is stochastic. The deterministic term has two components. The first is a "fading memory" component whose meaning becomes more clear if we introduce the relation

$$T_L = \frac{2\sigma_w^2}{C_0 \epsilon}. \quad (2)$$

Here  $T_L$  is the Lagrangian integral timescale. The value of  $C_0$  was chosen as 5.7. The second component of the deterministic term is a "drift correction" that accounts for the vertical inhomogeneity of turbulence. Equations similar to Eq. (1) provide the horizontal components of particle motion with  $(x, y)$ ,  $(\sigma_u, \sigma_v)$ , and  $(u, v)$  replacing  $z$ ,  $\sigma_w$ , and  $w$ , respectively.

The turbulence input parameters chosen for this study are

$$\sigma_w^2 = u_*^2 \left[ 1.6 \left( 1 - \frac{z}{h} \right)^{3/2} + F \left( \frac{z}{L} \right) \right] \quad (3a)$$

$$\sigma_u^2 = \sigma_v^2 = (\bar{U} \sigma_\theta)^2 \quad (3b)$$

$$\epsilon = \frac{u_*^3}{kz} \left[ \left( 1 + 3.7 \frac{z}{L} \right) \left( 1 - 0.85 \frac{z}{h} \right)^{3/2} + G \left( \frac{z}{L} \right) \right], \quad (4)$$

where  $F(z/L)$  and  $G(z/L)$  are atmospheric stability functions.

Boundary layer input parameters chosen for the MATHEW-ADPIC simulations of the experiment were as follows: The wind-direction fluctuation  $\sigma_\theta$ , based on measurements from towers and vertical soundings, was  $18^\circ$  at  $z = 0$  and  $12^\circ$  at  $z = h$ . The boundary layer height  $h$  was 300 m as determined from temperature profiles, a Monin-Obukhov length  $L$  of 10 m was based on bulk Richardson number measurements, and a constant surface roughness height  $z_0$  of 0.5 m was used over the domain. The ADPIC grid consisted of  $80 \times 80 \times 40$  cells of  $500 \text{ m} \times 500 \text{ m} \times 20 \text{ m}$  each in the  $x$ ,  $y$ , and  $z$  directions, respectively. Wind fields were updated hourly. Where measurements were taken at intervals of less than an hour—for example, 15-min measurements at the RFP tower—each data point in the interpolation run represented an hourly average and, when measurements were missing, the average was over those measurements that were present. For missing hourly measurements or for measurements taken at interval of greater than 1 h, data were temporally interpolated to the appropriate hour.

### 3. Observational results

#### a. Evolution of flow structure

Full lidar volume scans were taken nine times during the night of 4–5 February as shown in Table 2. Figure 3 shows analyses from six of these scans taken between midnight and 0400 MST for a level surface 2084 m

TABLE 2. Lidar volume scans (HRFR1).

Start time (MST)	Stop time (MST)	Comments
1948:14	1954:49	Partial scan, through $1.6^\circ$ elevation, due to lost lock
1954:49	2005:27	Partial scan
1. 2128:11	2147:18	Noisy data
2. 2212:55	2246:55	Good volume
3. 2310:21	2331:07	Lower angles are bad
2331:07	2339:50	Partial scans—lower angles only
4. 0021:22	0042:23	Bad shots at $1.6^\circ$ elevation
0109:09	0118:55	Partial; some bad beams at $1^\circ$ elevation
0118:55	0123:41	Partial scan, noisy data
5. 0127:55	0146:10	Good volume
6. 0205:33	0224:56	Good volume
7. 0249:24	0304:23	Good volume
8. 0340:07	0403:03	Good volume
9. 0447:18	0507:35	Signal is low

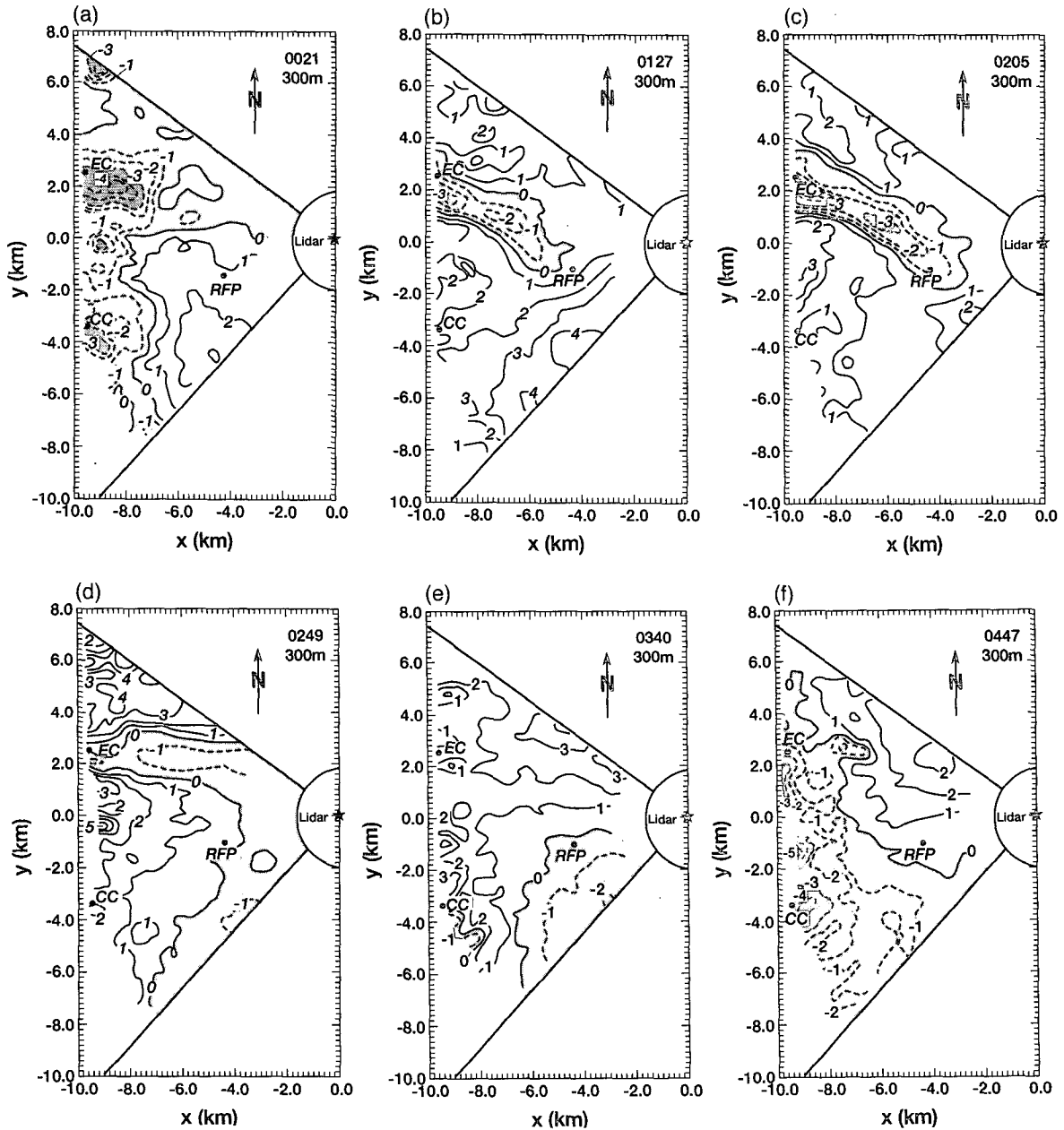


FIG. 3. Doppler lidar flow field for the 2084-m MSL level, representing a level surface 300 m above the lidar. Positive values indicate flow away from the lidar, which was at the location marked with a star. Shown are six time periods for the night 5 February 1991: (a) 0021 MST, (b) 0127 MST, (c) 0205 MST, (d) 0249 MST, (e) 0340 MST, and (f) 0447 MST. Contours are at 1  $m s^{-1}$  intervals. Light shading indicates negative velocities (flow toward the lidar), and dark shading, flow toward the lidar of over 3  $m s^{-1}$ . North is up and west to the left.

MSL, which represents the level 300 m above lidar level (ALL). The analyses are of the lidar radial wind field; negative values indicate flow toward the lidar, which in this case implies a westerly component. The sequence shows the formation, evolution, and demise of a major exit jet from Eldorado Canyon, and what seemed to be appearances and disappearances of an exit jet from Coal Creek Canyon. Differences in behavior

and structure of the efflux from the two canyons can be attributed to the fact that the airshed flowing into Eldorado Canyon is considerably larger and more complex than the airshed of Coal Creek.

Figure 3a shows that shortly after midnight, shallow exit jets (flow toward the lidar) were spilling out of both Eldorado Canyon (EC) and Coal Creek Canyon (CC). This was the last of four analyses (others were

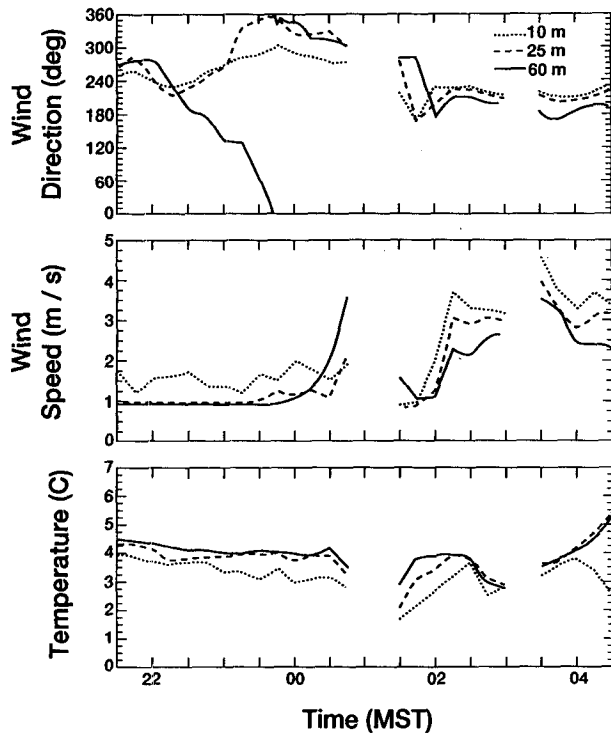


FIG. 4. Time series of wind direction and speed ( $\text{m s}^{-1}$ ) and temperature ( $^{\circ}\text{C}$ ) from three levels on the 61-m Rocky Flats tower for the night of 4–5 February 1991. Banta et al. (1993b) suggested that the increase in wind speed at 60 m and the accompanying decrease in temperature indicated around 0100 MST (despite the unfortunate lack of two observation reports) was a signature of the Eldorado jet bending southward over RFP. Each observation point represents a 15-min average.

taken at 2128, 2212, and 2317 MST) that all showed essentially the same pattern of flow from both canyons, indicating that conditions had not changed significantly during the time period between 2100 and 0020 MST. An hour later at 0127 MST (Fig. 3b), however, the Eldorado jet strengthened and extended southeasterly over the plains toward RFP, whereas the Coal Creek jet disappeared at this level. Another half hour later (at 0205 MST, Fig. 3c) the Eldorado Canyon jet seemed to completely dominate the flow over RFP. It was a narrow, strong jet less than 4 km wide even several kilometers from the mouth of the canyon, and data to the east of the lidar from vertical cross sections presented later in this section show that it remained a narrow jet well to the east of the lidar. After this time the jet began to decay, and by 0249 MST, 44 min after Fig. 3c, the Eldorado jet had turned to flow due east and had considerably diminished in intensity (Fig. 3d). By 0340 MST—about an hour later—the Eldorado Canyon exit jet completely vanished at this level (Fig. 3e). Interestingly, another hour after that, *both* the Eldorado and the Coal Creek jets reappeared (Fig. 3f), much as they had been before midnight. The growth

and decay of the Eldorado Canyon exit jet as a dominant entity over the RFP region thus took place in a 3-h period, and during that time significant structural changes were observed to occur over intervals of 30–45 min.

A few comments about Fig. 3 are necessary: 1) Mini-sodar and tower data at the mouth of Coal Creek Canyon showed a strong and persistent but very shallow jet with a maximum of  $6\text{--}8 \text{ m s}^{-1}$  at approximately 50 m above ground level (AGL) at all times between 2000 and 0500 MST (Coulter 1993, personal communication). Thus, the appearance and disappearance of the Coal Creek exit jet in Fig. 3 was at a level above this shallow, persistent westerly jet seen by the other instruments, and the transience actually represented a deepening and shallowing of the Coal Creek jet, rather than a complete formation and disappearance. 2) Tower data, for example, at the top and bottom of the RFP tower, often showed flow near the earth's surface decoupled (from a different direction—generally westerly or southwesterly at RFP) from the flow just above. This indicates katabatic surface flow occurring in a very shallow layer only a few tens of meters deep. At the RFP tower, Fig. 4 shows that the wind direction at 10 m AGL was at least  $40^{\circ}$  different from the 60-m direction from 2230 to 0145 MST. The flow at 10 m was also stronger and colder than at either level above. Levinson and Banta (1995) and Banta et al. (1995) similarly found a shallow katabatic layer on 7–8 February, another night with light ambient flow. 3) The similarity between this sequence at 300 m ALL and the

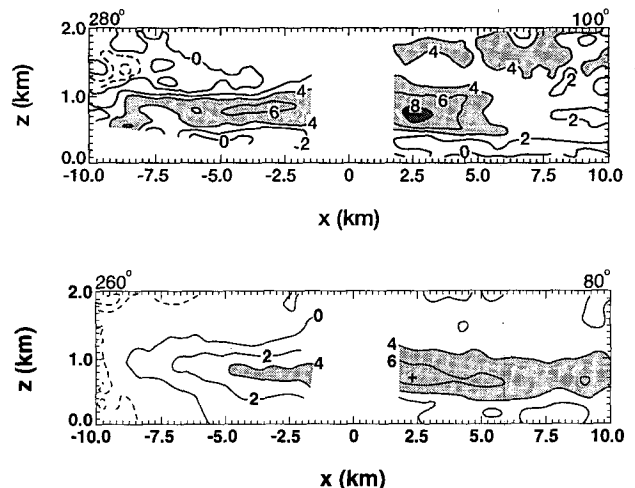


FIG. 5. Vertical cross sections of (nearly) westerly wind component from the Doppler lidar. (a) In the upper figure, left points toward  $280^{\circ}$  and the Eldorado Canyon mouth is to the left at a range of about 10 km. Lidar scan began at 0152 MST. (b) Lower figure, left is toward  $260^{\circ}$ , and scan began at 0151 MST. The cross indicates location of maximum flow speed of  $7.1 \text{ m s}^{-1}$ . In both panels lidar was located at (0, 0), and contour interval is  $2 \text{ m s}^{-1}$ . Light shading indicates where westerly flow is greater than  $4 \text{ m s}^{-1}$ ; dark shading indicates greater than  $8 \text{ m s}^{-1}$ .

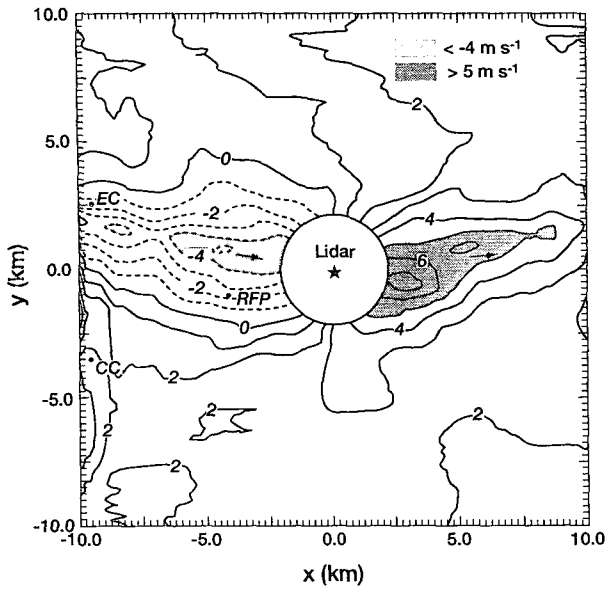


FIG. 6. Horizontal analysis of Doppler lidar data for the level surface 600 m ALL (2384 m MSL), constructed from vertical cross sections (as in Fig. 5) every 20° around the compass. North is up, west to the left, and lidar is in the middle at (0, 0). Contours are at 1 m s<sup>-1</sup> intervals, with positive values indicating flow away from the lidar.

sequence presented by Banta et al. (1993b) at 200 m ALL indicates that the Eldorado jet was not a shallow layer only a few tens of meters deep, but that it had to be significantly deeper than 100 m. This conclusion is reinforced by Elderkin and Gudiksen's (1993) analysis of lidar data of the 150-m ALL surface for 0205 MST, which showed a strong jet from Eldorado Canyon as in Fig. 3c. The jet flow at both 200 m and 150 m ALL exceeded 4 m s<sup>-1</sup>, somewhat stronger than the 3 m s<sup>-1</sup> at 300 m ALL shown in Fig. 3.

In addition to the volume scans, the lidar also performed vertical scans at constant azimuth (RHI scans), including a sequence of vertical slices around the compass every 20° that began at 0147 MST. Two such scans were at 260° and 280° azimuth (Fig. 5). The upper scan (280°), which points toward Eldorado Canyon (to the left in the figure), shows that the exit jet actually reached maximum speeds at approximately 700 m ALL, or 400 m above the level of the analyses in Fig. 3. Thus, the strongest part of the jet flowed aloft out of the mouth of the canyon, suggesting that the source of the cold air was farther back in the airshed, and thus farther back in the mountains [special analyses of these scans presented by Ruffieux et al. (1992) and Banta et al. (1995) support this view]. The jet seemed to die rather suddenly 5 km east of the lidar in the upper figure, but the lower figure shows that it persisted, although it actually bent somewhat to the north. This geometry is illustrated in

Fig. 6, which shows a level surface 600 m ALL. The figure was constructed from *all* the around-the-compass vertical scans, which included the two in Fig. 5. It shows that just before 0200 MST the Eldorado Canyon exit jet streamed eastward as a narrow, intense channel out onto the plains to the edge of the lidar's range, which was more than 20 km from the mouth of the canyon. Thus, at 500–700 m ALL, the jet did not diverge significantly in the horizontal after it flowed out of the canyon mouth. Analyses below 400 m ALL showed a more diffuse wind speed pattern, indicating that the jet at lower levels did diverge more than at upper levels. Maximum speeds at the lower levels appeared more to the east and southeast of the lidar than at 600 m ALL (Fig. 6).

Clarification of this complicated and somewhat confusing picture comes from further analysis of the 0205 MST volume scan (the one from which Fig. 3c was analyzed) by Banta et al. (1995), who made vertical cross sections running north–south across the mouth of Eldorado Canyon, between the canyon and RFP. These cross sections reveal a multiple-jet structure with two major jets: an upper jet at about 600 m ALL and a lower jet below 300 m. The jets do not stack vertically, but the upper jet lies to the north of the lower. We are continuing to analyze this jet structure in greater detail.

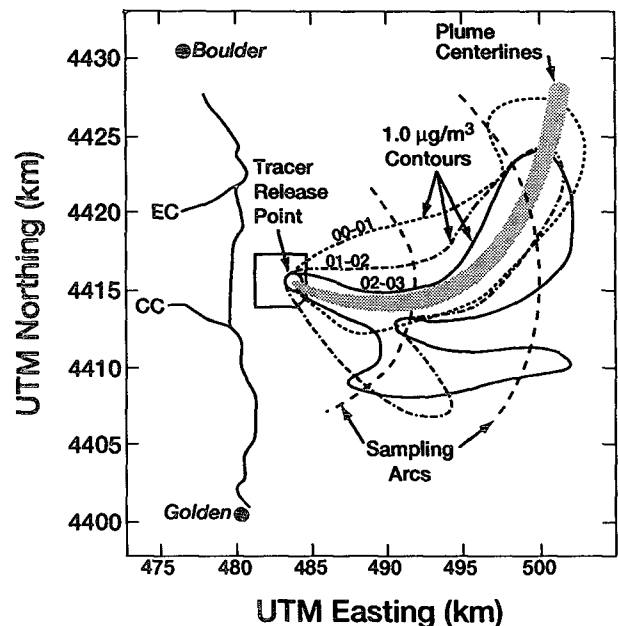


FIG. 7. Sulfur hexafluoride (SF<sub>6</sub>) tracer concentration data in the vicinity of RFP on 5 February 1991 for three sample averaging periods: 0000–0100 MST (dotted), 0100–0200 MST (dashed), and 0200–0300 MST (solid). Plume outline is indicated by the 1 g m<sup>-3</sup> contour (after Elderkin and Gudiksen 1993). Centerline represents location of maximum concentrations, which was at the same samplers for all three time periods as indicated in the text and in Fig. 2.

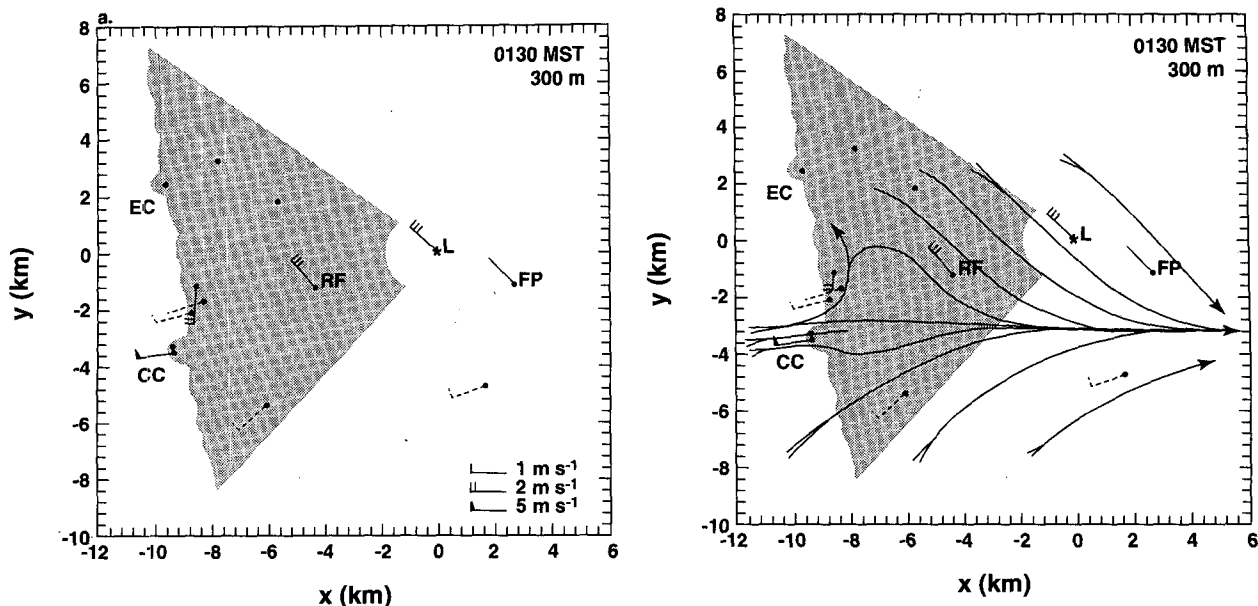


FIG. 8. (a) Wind data from ASCOT instrument array at 0130 MST for the 300-m ALL surface. Solid wind bars indicate upper-air data on this surface, and dotted wind bars indicate tower data that are above or below the surface. Each barb represents 1 m s<sup>-1</sup>. Shading indicates region of the lidar scans in Fig. 3. The following sites are indicated: Eldorado Canyon (EC), Coal Creek Canyon (CC), Rocky Flats tower/rawinsonde (RF), Doppler lidar (L), and Filtration Plant (FP). The three dots to the north of RF (and east of EC) show the three potential locations from which the tethered balloon, normally operated at the EC location, could be launched, depending on wind speed. At 0100 and 0200 MST on this night, however, the winds were too strong at all three sites, and no balloon could be launched. (b) Streamline analysis of wind data in (a).

#### b. Tracer movement

Because the jet is strongest aloft, it would have been most revealing to see the effects of an elevated release, but during this study all tracer releases were from the surface. Results from the evening of 4–5 February during the time of influence of the Eldorado jet are shown in Fig. 7, which shows the plume outline as indicated by the 1  $\mu\text{g m}^{-3}$  contour (from Shearer 1992). During the period 0000–0100 MST the tracer was all advected to the east and east-northeast, with no evidence of southeasterly transport. This behavior (i.e., without influence from the Eldorado Canyon jet) is consistent with the flow field as analyzed by the diagnostic models from the conventional meteorological data and UHF profilers. Between 0100 and 0200 MST, Fig. 7 still shows a peak to the east and east-northeast, but another lobe of the tracer plume is indicated to the southeast at the 8-km ring. By 0200–0300 MST, the southeasterly lobe showed up at both the inner and outer sampler rings. Thus, tracer data did show evidence of transport to the southeast, indicating the effects of the Eldorado exit jet, even for surface sampling and a surface release.

An interesting observation regarding this dataset is that the maximum tracer concentration at the 16-km ring was always at the same sampler on this night, and at the 8-km ring, the maximum concentration was noted at the same sampler until 0400, when the peak shifted one sampler to the north (Shearer 1992). The maxi-

um at 8 km occurred almost due east of the release site, and at 16 km it was more east-northeasterly, indicating a bend in the plume. This behavior provides insight into the nature of the flow that carried the main plume—this flow was strongly guided by topography. Thus, under the light synoptic flow conditions on this night, the flow transporting the main plume was most likely a shallow katabatic layer that followed a shallow gully.

### 4. Modeling results

#### a. Wind field

Data available during the night of 4–5 February 1991 from instrumented towers, rawinsonde, tether-sonde, Doppler minisodars, and UHF profilers are shown in Fig. 8a for 0130 MST. Upper-air data are interpolated to a level surface 2084 m MSL to correspond to the lidar analyses at 300 m ALL (Fig. 3). Tower data (dashed flags), which are not at the level, are given for the tower-instrumentation height nearest the level. For stations near the foothills, the data were 0–200 m below this surface, and one tower, the BR (Bartlett's Ranch) site, was about 400 m below it. This represents a rather dense array of instruments, with observations every 3–5 km over the limited area, at least compared with what is normally available for dispersion modeling applications. The figure is very similar

to data 100 m lower at the 1984-m surface presented by Banta et al. (1993b).

Figure 8b, a streamline analysis of the data in Fig. 8a, shows generally northwesterly flow to the north of RFP converging with west-southwesterly flow to the south. The combined flows then continued to the east, where they met the larger-mesoscale, southerly drainage from the South Platte River valley. This overall picture of converging northwesterly and west-southwesterly flow over RFP agrees with diagnostic model output based on the same dataset for the same time period augmented with FSL mesonet data. For example, Fig. 9 shows MATHEW wind fields for 0100 MST, with northwesterly flow coming out of Eldorado Canyon and west-southwesterly flow to the south of RFP.

*b. Tracer concentration*

MATHEW-ADPIC was run based on the available data excluding the lidar data. Results are shown in Fig. 10 for the 8-km and the 16-km rings, with actual tracer data also plotted. Both model and tracer data show a peak in tracer concentration to the east. The data also indicate a peak to the southeast as in Fig. 7, but this peak was not picked up by the model output. Thus, the diagnostic models seemed to do a good job of picking up the easterly peak in tracer concentration produced by the predominantly westerly katabatic flow layer at the surface, but they did not show the secondary southeasterly peak at all.

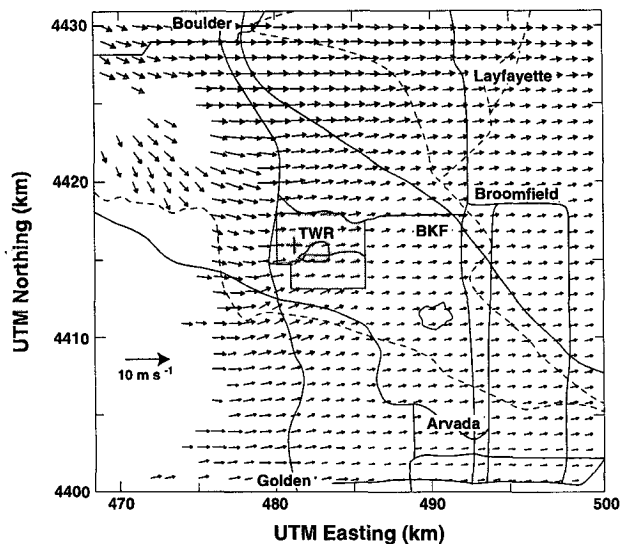


FIG. 9. MATHEW wind field analysis at 0100 MST for a portion of the simulation domain. Wind arrows indicate the flow at 40 m AGL. Blank regions to the left of the figure are where the topography (mountains) protrude above the top of the domain. Square indicates RFP boundary, and the cross (+) marked "TWR" indicates RFP tower location.

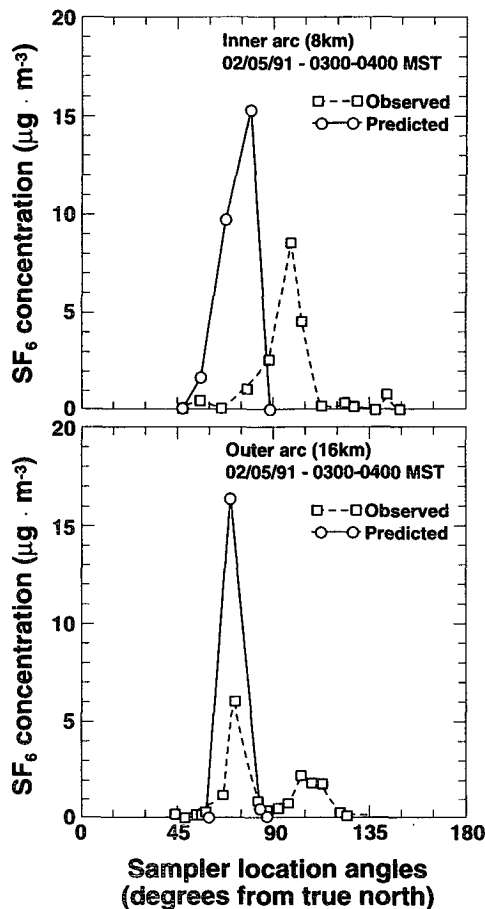


FIG. 10. Sulfur hexafluoride (SF<sub>6</sub>) concentration data as calculated by MATHEW-ADPIC model and as measured. Abscissa is the angular distance in degrees from north of each sampler in the 8- and 16-km rings. Solid line indicates model calculation, and dotted line, concentrations observed by the sampling network.

*c. Discussion*

Tracer measurements show two peaks in concentration, one to the east and east-northeast and another to the southeast. The first corresponds to transport by a thin katabatic layer of surface flow that followed the topography. The second resulted from transport by the northeasterly Eldorado exit jet sweeping southward over RFP for 2–3 h during the early morning. Banta et al. (1995) hypothesized that the mechanism carrying the tracer material upward into the jet was periodic surfacing of the strong, northwesterly flow from the Eldorado jet by intermittent turbulence in the stable surface layer. This mechanism also later carried tracer downward to the surface samplers.

The diagnostic model represented the primary maximum in concentration rather well, although the direction was off by approximately 25° at the 8-km arc. This agreement was most likely because the experiment was dominated by surface events: tracer was released at the

surface, carried by shallow surface flows, and sampled at the surface. Thus, the network of wind observations, which was also densest at the surface, sampled the surface flow adequately. If the tracer had been released above the surface and above the katabatic flow layer, and if the sampling had been higher above the ground, the agreement would have probably been poorer.

Results of this study suggest ways in which dispersion modeling in complex terrain can be improved. MATHEW-ADPIC was run for many of the other experimental days in February 1991 in addition to the present case study. Results consistently indicated that the direction of the modeled and observed tracer plume centerlines relative to the source disagreed by angles that were large compared with the plume width. This implies that the errors in the dispersion estimates were due primarily to errors in the advecting wind field rather than to errors in the turbulent diffusion calculations, in agreement with statements made in the introduction. In turn, this implies that optimizing and fine-tuning the diffusion scheme is less critical than accurately modeling the wind field.

Thus, major improvements in complex-terrain dispersion modeling will depend primarily on improving the modeled wind field. Obviously, the model must have fine enough resolution in space and time, but also either the observations must be at sufficiently fine resolution, or the instruments must be strategically placed to sample flow features that have a significant effect on transport. Because mesonet stations and other instruments are expensive to deploy, it seems more likely in applications dealing with a fixed site that the judicious siting of instruments is the more viable option. Banta et al. (1993b) suggest ways in which this could be done, including a careful study of the finescale topography, and a short-term field program. The aim of this program would be to obtain a fine-resolution dataset of the local flow, either by a high-density mesonet, which would include some vertical sounding information from tethered balloons, profilers, or rawinsondes, or by active remote-sensing instrumentation such as the Doppler lidar. Our experience at Rocky Flats shows that such a field program is much more effective when coupled with a tracer experiment.

This study has emphasized the role of a diagnostic wind field model in determining dispersion, but diagnostic schemes in complex terrain have little value in predicting future wind and concentration fields, because of their reliance on observed data, and because the winds are constantly changing. Three-dimensional dynamic mesoscale models and the computers they run on are becoming faster, and they may become useful for real-time forecasting of dispersion over complex topography. Currently Bossert and Poulos (1993), Poulos and Bossert (1995), and Fast (1995) have used the RAMS model rather successfully in research mode with nesting in three dimensions to simulate the Rocky Flats case described in this study.

The question of whether these models could be used as real-time tools depends to a large extent on what range of scales they need to simulate—that is, on one hand how fine the resolution must be, and on the other, how large a domain they must cover. From this study it is apparent that small-scale features of less than 2-km width and the topography that produces them must be adequately represented. On the larger-scale end, this and other studies have shown that some larger topographically forced systems can form, change, or dissipate over time periods of an hour or so. These include, for example, the flows from the South Boulder Creek basin that drains through Eldorado Canyon as discussed in this study and in Banta et al. (1993b) and so-called Denver cyclones and other terrain-forced mesoscale vortices (Levinson and Banta 1995). Because these systems (which occur on a scale somewhat larger than the dispersion domain of interest) change so rapidly, treating their measurements as boundary conditions or assimilation data for a smaller-scale dispersion model would limit the capability of the model to forecast beyond available data. However, since they are organized and deterministic rather than random turbulence, in principle their evolution should be predictable. Thus, in the horizontal, a model must have a resolution of less than 1 km, but the domain must reach 100 to a few hundred kilometers. This is within the range of current nested models as research tools, but to be useful for 2–12 h forecasts as an emergency-response tool, models will probably need to be able to make such a run in an hour or less.

## 5. Conclusions

The most surprising finding from the 4–5 February nighttime study was the dominance of the Eldorado Canyon exit jet over the RFP region for a 3-h period in the middle of the night. We expected Coal Creek Canyon flow to have the major influence on the RFP region because of its proximity and because Coal Creek itself flows past RFP, whereas South Boulder Creek, which flows out of Eldorado Canyon, turns north toward Boulder. Although Coal Creek does often affect flow over RFP during the night (Hubbe 1993), it is apparent that for the period between 0000 and 0300 MST 5 February the powerful exit jet from Eldorado Canyon flowed strongly eastward and southeastward across the essentially north–south gullies and took control of the flow over RFP. The present study addressed three questions concerning: 1) the structure and evolution of this small-scale feature, 2) its effect on dispersion of material released at RFP, and 3) the implications of these effects on modeling this dispersion.

First, ETL's Doppler lidar found a narrow, 3–4 m s<sup>-1</sup> stream approximately 2 km wide between the Eldorado Canyon mouth and RFP. This exit flow was one of two major local flow systems forced by cooling at the earth's surface, the other being a thin katabatic-

flow layer next to the surface, which was strongly guided by topography. During the strongest stage of the jet, lidar analyses showed a multiple-jet structure emerging from the Eldorado Canyon mouth. The upper branch remained strong and narrow (<4 km wide) for as far as the lidar could see—that is, more than 20 km from the canyon mouth. The emergence aloft from a canyon of already-strong flow implies a source farther back in the mountain valleys that feed into the canyon. The jet changed rapidly in time, as major structural changes took place over time periods of 30–45 min or less.

Second, the jet did have an effect on the advection of tracer material released at RFP. Although the primary tracer plume was carried to the east through east-northeast by the katabatic layer next to the surface, secondary plumes appeared to the southeast. Tracer material released at the surface leaked upward through the stable katabatic-flow layer into the lower portion of the northwesterly Eldorado jet, which carried it to samplers in the 8- and 16-km sampling rings. The jet was thus responsible for secondary plumes, which appeared to the southeast of RFP.

Third, the main effect of the Eldorado canyon jet on modeling dispersion from RFP was its absence from the observations and thus from the modeled advecting wind field. The true nature of the Eldorado Canyon jet—narrow, meandering, and strong relative to other flow in the area—was not captured by the measurement network, even though the network was rather dense compared with what is often available for diffusion applications (Banta et al. 1993b). As a result, dispersion model runs based on these data did not reflect the peak in tracer concentrations to the southeast of RFP. Hourly sampling was insufficient to capture the 30–45-min changes in the structure of the flow. Although the absence of the jet feature might have a relatively minor effect for hazardous contaminants that require long exposure times to produce ill effects, it could be important for toxic substances released by accident or in wartime.

The results in this study highlighted two other issues. The first is that, because of the strong vertical layering and horizontal variability, contaminants released at different heights or at slightly different locations in the horizontal could easily be advected along widely divergent trajectories (Banta et al. 1993b). The second is that some of the variability in hourly averaged winds at a fixed station was produced by organized flow structures. For example, the increase in wind speed at the upper anemometer of the RFP tower (Fig. 4), which was attributed to the Eldorado jet, would contribute significantly to the variance in the mean hourly wind. Because this variability was produced by an organized, potentially predictable feature, and not from random turbulence, its effect should be reflected in the modeled advecting wind field rather than in the turbulent diffu-

sion calculation. This could be done by averaging over time periods of less than 1 h.

Achieving the goal of improving dispersion calculations in complex terrain thus depends in many cases on improving the representation of small-scale features in the modeled wind field. Certainly one of the major obstacles is the lack of adequate documentation of flow features that need to be modeled, based on fine-resolution measurements. Even if the models did reproduce these features faithfully, the lack of observations confirming the model results would still leave the reality of the simulated features in doubt. These shortcomings could be overcome by the availability of finescale observational datasets, which are becoming available through scanning, active remote sensing systems such as the Doppler lidar described in this paper.

*Acknowledgments.* This research was sponsored by the U.S. Department of Energy with Michael Riches as technical contract monitor, as a part of the Atmospheric Studies in Complex Terrain (ASCOT) program. We thank Bill Neff, Dave Levinson, Dick Cupp, and Ron Willis for their roles in experiment design, data acquisition, and data analysis, and our colleagues Charles Elderkin, John Hubbe, Clark King, Rich Coulter, Bill Clements, Chris Doran, Mike Smith, John Ciolek, Don Shearer, and others in ASCOT for interesting and helpful discussions on issues discussed in this paper, and access to specialized datasets. We also appreciate helpful reviews of the manuscript by Clark King and Dan Wolfe.

## REFERENCES

- Banta, R. M., and L. D. Olivier, 1991: Doppler lidar observations of air flow in the Grand Canyon. *Proc. 84th Annual Meeting, Air and Waste Management Association, Vol. 2, Atmospheric Monitoring and Measurement*, Pittsburgh, PA, Air and Waste Management Association, Paper 91-47.11, 1–16.
- , —, E. T. Holloway, R. A. Kropfli, B. W. Bartram, R. E. Cupp, and M. J. Post, 1992: Smoke-column observations from two forest fires using Doppler lidar and Doppler radar. *J. Appl. Meteor.*, **31**, 1328–1349.
- , —, and D. H. Levinson, 1993a: Evolution of the Monterey Bay sea-breeze layer as observed by pulsed Doppler lidar. *J. Atmos. Sci.*, **50**, 3959–3982.
- , —, and P. H. Gudiksen, 1993b: Sampling requirements for drainage flows that transport atmospheric contaminants in complex terrain. *Radiat. Prot. Dosim.*, **50**, 243–248.
- , —, W. D. Neff, D. H. Levinson, and D. Ruffieux, 1995: Influence of canyon induced flows on flow and dispersion over adjacent plains. *Theor. Appl. Climatol.*, **52**, 27–42.
- Bossert, J. E., and G. S. Poulos, 1993: Numerical simulation of atmospheric dispersion in the vicinity of the Rocky Flats Plant. *Proc. Topical Meeting on Environmental Transport and Dosimetry*, Charleston, SC, Amer. Nuclear Soc., 75–78.
- Browning, K. A., and R. Wexler, 1968: The determination of kinematic properties of a wind field using Doppler radar. *J. Appl. Meteor.*, **7**, 105–113.
- Clark, T. L., W. D. Hall, and R. M. Banta, 1994: Two- and three-dimensional simulations of the 9 January 1989 severe Boulder windstorm: Comparison with observations. *J. Atmos. Sci.*, **51**, 2317–2343.

- Doran, J. C., 1993: An overview of the ASCOT program. *Proc. Topical Meeting on Environmental Transport and Dosimetry*, Charleston, SC, Amer. Nuclear Soc., 75-78.
- Ecklund, W. L., D. A. Carter, and B. B. Balsley, 1988: A UHF wind profiler for the boundary layer: Brief description and initial results. *J. Atmos. Oceanic Technol.*, **5**, 432-441.
- , D. A. Carter, B. B. Balsley, P. A. Currier, J. L. Green, B. L. Weber, and K. S. Gage, 1990: Field tests of a lower tropospheric wind profiler. *Radio Sci.*, **25**, 899-906.
- Elderkin, C. E., and P. H. Gudiksen, 1993: Transport and dispersion in complex terrain. *Radiat. Prot. Dosim.*, **50**, 265-271.
- Fast, J. D., 1995: Mesoscale modeling and four-dimensional data assimilation in areas of highly complex terrain. *J. Appl. Meteor.*, **34**, 2762-2782.
- Filliger, P., and H. Wanner, 1986: Transport and dispersion of air pollutants in a slope wind area. *Extended Abstracts, Fifth Joint Conf. on Applications of Air Pollution Meteorology*, Chapel Hill, NC, Amer. Meteor. Soc., 269-272.
- Hubbe, J. M., and K. J. Allwine, 1993: Mesoscale meteorological measurements characterizing complex flows. *Proc. Topical Meeting on Environmental Transport and Dosimetry*, Charleston, SC, Amer. Nuclear Soc., 47-51.
- Hunt, J. C. R., R. J. Holroyd, D. J. Carruthers, A. G. Robins, D. D. Apsley, F. B. Smith, and D. J. Thompson, 1991: Developments in modeling air pollution for regulatory uses. *Proc. 18th NATO-CCMS ITM on Air Pollution Modeling and its Applications*, H. van Dop, and D. G. Steyn, Eds., Plenum Press, 17-59.
- Lange, R., 1978: ADPIC—A three dimensional particle-in-cell model for the dispersal of atmospheric pollutants and its comparison to regional tracer studies. *J. Appl. Meteor.*, **17**, 320-329.
- , 1985: Relationship between model complexity and data base quality for complex terrain tracer experiments. Ph.D. dissertation, University of California, Davis, 140 pp.
- , 1989: Transferability of a three-dimensional air quality model between two different sites in complex terrain. *J. Appl. Meteor.*, **28**, 665-679.
- , 1992: Modeling the dispersion of tracer plumes in the Colorado Front Range boundary layer during night- and day-time conditions. Preprints, *10th Symp. on Turbulence and Diffusion*, Portland, OR, Amer. Meteor. Soc., J163-J166.
- , 1993: Application of an atmospheric dispersion model to simulated pollutant releases in the Colorado Front Range. *Proc. Topical Meeting on Environmental Transport and Dosimetry*, Charleston, SC, Amer. Nuclear Soc., 85-88.
- Levinson, D. H., and R. M. Banta, 1995: Observations of a terrain-forced mesoscale vortex and canyon drainage flows along the Front Range of Colorado. *Mon. Wea. Rev.*, **123**, 2029-2050.
- May, P. T., K. P. Moran, and R. G. Strauch, 1989: The accuracy of RASS temperature measurements. *J. Appl. Meteor.*, **28**, 1329-1335.
- Mikkelsen, T., and F. Desiato, 1993: Atmospheric dispersion models and pre-processing of meteorological data for real-time application. *Radiat. Prot. Dosim.*, **50**, 205-218.
- Neff, W. D., J. R. Jordan, J. E. Gaynor, D. E. Wolfe, W. L. Ecklund, D. A. Carter, and K. S. Gage, 1991: The use of 915-MHz wind profilers in complex terrain and regional air quality studies. Preprints, *Seventh Joint Conf. on Applications of Air Pollution Meteorology with AWMA*, New Orleans, LA, Amer. Meteor. Soc., J230-J233.
- Neiman, P. J., R. M. Hardesty, M. A. Shapiro, and R. E. Cupp, 1988: Doppler lidar observations of a downslope windstorm. *Mon. Wea. Rev.*, **116**, 2265-2275.
- Post, M. J., and R. E. Cupp, 1990: Optimizing a pulsed Doppler lidar. *Appl. Opt.*, **29**, 4145-4158.
- Poulos, G. S., and J. E. Bossert, 1995: An observational and prognostic numerical investigation of complex terrain dispersion. *J. Appl. Meteor.*, **34**, 650-669.
- Rasmussen, R. M., M. K. Politovich, J. Marwitz, W. Sand, J. McGinley, J. Smart, R. Pielke, S. Rutledge, D. Wesley, G. Stossmeister, B. Bernstein, K. Elmore, N. Powell, E. Westwater, G. Stankov, and D. Burrows, 1992: Winter Icing and Storms Project. *Bull. Amer. Meteor. Soc.*, **73**, 951-974.
- Ruffieux, D., W. D. Neff, and R. M. Banta, 1992: Visualization of flows channelled in canyons using Doppler lidar data. Preprints, *Sixth Conf. on Mountain Meteorology*, Portland, OR, Amer. Meteor. Soc., 111-115.
- Shearer, D. L., 1992: *Atmospheric Tracer Data from the Rocky Flats 1991 Winter Validation Study*. Vol. 1, *Night Experiments*. LA-UR-92-2507, ASCOT-92-1, Los Alamos National Laboratory, University of California, Los Alamos, NM, 280 pp.
- Sherman, C. A., 1978: A mass-consistent model for wind fields over complex terrain. *J. Appl. Meteor.*, **17**, 312-319.
- Sullivan, T. J., J. S. Ellis, C. S. Foster, K. T. Foster, R. L. Baskett, J. S. Nasstrom, and W. S. Schalk, 1993: Atmospheric Release Advisory Capability: Real-time modeling of airborne hazardous materials. *Bull. Amer. Meteor. Soc.*, **74**, 2343-2361.
- Whiteman, C. D., 1990: Observations of thermally developed wind systems in mountainous terrain. *Atmospheric Processes over Complex Terrain*, W. Blumen, Ed., *Meteor. Monogr.*, Amer. Meteor. Soc., No. 45, 5-42.
- Wolfe, D. E., D. C. Welsh, and C. D. Whiteman, 1991: Wind structure within the Grand Canyon as observed by a low-level wind profiler. *Proc. 84th Annual Meeting, Air and Waste Management Association*, Pittsburgh, PA, AMWA, Paper 91-85.2, 1-14.
- , B. L. Weber, D. B. Wertz, J. E. Gaynor, and J. P. Ye, 1993: Comparisons of quality control methods for low-level wind profiler data. Preprints, *Eighth Symp. on Meteorological Observations and Instrumentation*, Anaheim, CA, Amer. Meteor. Soc., 257-263.